Manuscript title: **Plantar soft tissue characterization using Reverberant Shear Wave Elastography: a proof-of-concept study**

Authors' names: Stefano E. Romero[1], Roozbeh Naemi[2], Gilmer Flores[1], David Allan[2], Juvenal Ormachea[1,3], Evelyn Gutierrez[1], Fanny L. Casado[4], Benjamin Castaneda[1]

Institutional affiliations:
[1] Laboratorio de Imagenes Medicas, Pontificia Universidad Catolica del Peru, San Miguel, Lima, Peru
[2] Centre for Biomechanics and Rehabilitation Technologies, School of Health, Science and Wellbeing, Staffordshire University, Stoke-on-Trent, UK
[3] Department of Electrical and Computer Engineering, University of Rochester, Rochester, NY USA
[4] Instituto de Ciencias Omicas y Biotecnologia Aplicada, Pontificia Universidad Catolica del Peru, San Miguel, Lima, Peru

Corresponding author:
Stefano Romero
Pontificia Universidad Catolica del Peru
Av. Universitaria 1801, San Miguel
Lima 32, Peru
Phone: (51) 626-2000 - 4662
Email: sromerog@pucp.pe

Abstract

Plantar soft tissue stiffness provides relevant information on biomechanical characteristics of the foot. Therefore, appropriate monitoring of foot elasticity could be useful for diagnosis, treatment, or healthcare of people with complex pathologies such as diabetic foot. In this work, the reliability of reverberant shear wave elastography (RSWE) applied to plantar soft tissue was investigated. Shear wave speed (SWS) measurements were estimated at the plantar soft tissue at the first metatarsal head, the third metatarsal head and the heel from both feet in five healthy volunteers. Experiments were repeated for a test–retest analysis with and without the use of gel pad using a mechanical excitation frequency range between 400 and 600 Hz. Statistical analysis was performed to evaluate the reliability of the SWS estimations. In addition, the results were compared against those obtained with a commercially available shear wave-based elastography technique, supersonic imaging (SSI). The results indicate a low coefficient of variation for test–retest experiments with gel pad (median: 5.59%) and without gel pad (median: 5.83%). Additionally, the values of the SWS measurements increase at higher frequencies (median values: 2.11 m/s at 400 Hz, 2.16 m/s at 450 Hz, 2.24 m/s at 500 Hz, 2.21 m/s at 550 Hz and 2.31 at 600 Hz) consistent with previous reports at lower frequencies. The SWSs at the plantar soft tissue at the first metatarsal head, third metatarsal head and heel were found be significantly ($p<0.05$) different, with median values of 2.42, 2.16 and 2.03 m/s, respectively which indicates the ability of the method to differentiate between shear wave speeds at different anatomical locations. The results indicated better elastographic signal-to-noise ratios with RSWE compared to SSI because of the artefacts presented in the SWS generation. These preliminary results indicate that the RSWE approach can be used to estimate the plantar soft tissue elasticity, which may have great potential to better evaluate changes in biomechanical characteristics of the foot.

KEYWORDS: Elastography, Shear Wave, Ultrasound, Reverberant shear wave field, Plantar soft tissue

INTRODUCTION

Plantar soft tissue is the first area of the foot to be in contact with the ground during walking or running. Concentration of mechanical stress on the weight-bearing sections of the plantar soft tissue may generate histological changes that modify the biomechanical properties, leading to the deterioration of the structure of the foot. In middle-aged and older people, this could generate foot pain and nail and joint problems. For instance, Hill et al. (2008), reported that 20% of people in their study had foot pain, aching or stiffness, with a high prevalence in those classified as obese. The more complex pathologies such as diabetes could result in ulcerations or amputations. In that sense, diabetes foot is one of the most common consequences of diabetes disease progression (Cárdenas et al., 2015). This condition occurs as a result of damage to the nervous system as in peripheral neuropathy or ischemia (Pendsey, 2010). Broadly speaking, improper foot care could lead to injuries, infections and ulcerations, but diabetic patients are at greatest risk of foot amputation. While there is no consensus on the mechanism underlying the stages of deterioration in diabetic foot, some studies relate this condition to mechanical properties (Chao et al., 2011; Chatzistergos et al., 2014). Additionally, previous studies that used clinically viable methods such as strain elastography (SE) have reported a relationship between the mechanical properties of the plantar soft tissue in people with diabetes and the risk of ulceration (Naemi et al. 2016a, 2016b, 2017). However, in SE, strain rate dependency and the amount of force applied to the tissue as a viscoelastic material can affect the measurements of stiffness (Naemi and Chockalingam 2013; Naemi et al. 2016a, 2016b). Also, the non-linearity of the soft tissue mechanical behavior can be the reason for the major discrepancies in results in compression elastography.

Shear wave ultrasound elastography is another non-invasive method used to assess soft tissue stiffness. Shear wave elastography (SWE) deserves particular focus because of its capacity to provide quantitative data (Sigrist et al., 2017) and has been successfully used for tissue characterization (Hoyt et al. 2008; Gonzalez et al. 2018; Chiu et al. 2020; Machado et al. 2020; Hsu et al. 2021). Shear wave speed (SWS) has been used to assess the in vivo non-linear mechanical behavior of the heel pad with a commercially available SWE method (Chatzistergos et al., 2018). However, this application is limited as unidirectional shear wave propagation is not fully achieved because plantar soft tissue consists of a multilayer structure where, close to the bone, it generates excess reflections from its surface (Lin et al. 2017a, ; Wu et al. 2018). The novel elastography technique based on the application of a reverberant shear wave field (Parker et al., 2017,Parker et al., 2011) leverages wave reflections produced by internal inhomogeneities, organ boundaries, hard structures and physiological activity through application of multiple external vibration sources. Ormachea et al. (2018) verified the clinical feasibility of its use in breast and liver tissue using a multifrequency harmonic signal and compared it against a single-tracking-location acoustic radiation force impulse method. Later, Zvietcovich et al. (2019) advanced the physical model to consider multiple transversal polarizations of shear waves.

A gel pad is a common, flexible, disposable and easy-to-use ultrasound standoff that facilitates visualization of near-field areas (Klucinec, et al., 1996). Additionally, considering the complex foot anatomy, using a gel pad could make it easier to position the transducer at a correct angle parallel to the foot section in the acquisition (Yablon et al., 2013). While in previous studies no differences in the transmitted energy to the tissue using a gel pad was reported, given the applications of gel pads in musculoskeletal ultrasound, the comparison between reverberant shear

wave elastography (RSWE) and commercially available ultrasound while using a gel pad also needs to be investigated.

The main objective of this study was to investigate the reliability of using RSWE to measure SWS at the sole of the foot of healthy individuals. The secondary objective was to compare the values of SWS in plantar soft tissue obtained using RSWE with those obtained using commercially available shear wave ultrasound elastography equipment.

METHODS

Volunteer enrolment and data acquisition

Five healthy volunteers were recruited under the requirements of informed consent to the approved Research Protocol No. 021-2019 from the Research Ethics Committee at Pontificia Universidad Catolica del Peru (PUCP) and Staffordshire University. The age of the volunteers ranged between 27 and 44 years, and body mass index (BMI) ranged between 26.5 and 31.6 Kg/m^2. The experiments were performed at the Laboratorio de Imagenes Medicas at PUCP and at the Centre for Biomechanics and Rehabilitation Technologies at Staffordshire University. The participants were placed in a supine position on a wheeled stretcher with their feet positioned at the edge of the bed. Images were acquired using a linear array L11-4v (frequency = 9 MHz) operated by a Vantage 64LE (Verasonics, Kirkland, WA, USA) ultrasound system using plane wave mode acquisition. In addition, a frequency sample of 5 KHz, imaging field of view of 3 cm and spatial resolution of 86 µm were used. A graphic user interface based on MATLAB (Version 2019b, The MathWorks, Inc., Natick, MA, USA) was used to acquire the data. A set of driven speakers (Misco, Pleasanton, CA, USA) were placed onto the medial and lateral malleoli of the ankle to generate the reverberant shear wave field. Speakers were powered using an external amplifier (Denon Electronics, Mahwah, NJ, USA). Images from the first metatarsal head (MH), third MH and heel area of both

feet were acquired (Fig. 1). The acquisitions were performed with or without a gel pad and by applying ultrasound gel directly onto each foot. After identifying and centering the first MH, third MH and apex of the calcaneus for the heel pad (Naemi et al. 2016a, 2016b), the speakers emitted a multi-frequency audio track with 400, 450, 500, 550 and 600 Hz. The MATLAB script used to control the ultrasound probe indicates to the operator when the measurement has been completed. Next, the volume of the speakers was turned down. Three measurements were performed per location for each foot.

Data processing

Following the framework of Ormachea et al., (2018), offline processing was performed after Doppler US data were acquired. A Loupas algorithm (Loupas et al., 1995) was used to generate a 3-D matrix to estimate the particle velocity produced by the vibration. A temporal filter with a bandwidth of 20 Hz centered on each vibration frequency was applied. Additionally, a bandpass spatial filter with a wavenumber range of $\left[\frac{2\pi f_v}{c_h}; \frac{2\pi f_v}{c_l}\right]$ was applied considering that $f_v$is the vibration frequency and c_h and c_l are 0.7 m/s and 5 m/s, respectively. This range was chosen to avoid outliers in the SWS estimation based on the approximated stiffness range expected in plantar soft tissue (e.g., heel pad) according to previous studies (Lin et al. 2017a; Wu et al., 2018).

Shear Wave Speed Estimation

A 7.7 x 15.4 mm^2 moving kernel was used to estimate the local wavenumber to ensure at least the half-maximum wavelength of the signal in the entire process. The lateral profile from the normalized 2-D autocorrelation of particle velocity was extracted and fitted to its corresponding theoretical function (Zvietcovich et al., 2019) as in:

$$B_{v_z v_z}(\Delta t, \Delta \varepsilon_x) = V_{RMS}^2 \cos(\omega_0 \Delta t) \left[\frac{j_0(k\Delta\varepsilon_x)}{2} - \frac{j_1(k\Delta\varepsilon_x)}{2k\Delta\varepsilon_x} \right] \quad (1)$$

where $B_{v_z v_z}$ is the normalized 2-D autocorrelation, Δt is the time-difference, $\Delta\varepsilon_x$ is the displacement along the x-axis, ω_0 was the angular vibration frequency, $V_{RMS}^2 \cos(\omega_0 \Delta t)$ is the real part of the squared particle velocity magnitude, j_0 and j_1 are the spherical Bessel functions of the zero and first order, respectively; and k is the local wave number.

As Fig. 2 illustrates, only a lateral range from –2 to 2 mm, including the central lobe, was considered to avoid inaccurate results (Flores et al. 2020). Additionally, the coefficient of determination (R^2) was calculated as a goodness-of-fit parameter considering values from a minimum threshold of 0.7. After that, the resultant SWS was calculated as:

$$c_s = \frac{2\pi f_v}{k} \quad (2)$$

where c_s is the SWS.

The regions of interest (ROIs) were selected considering the outermost layer of the skin (epithelium) and the top of the corresponding anatomical landmark for each location. For analysis purposes, the mean value of the SWS from the ROI was evaluated. Fig. 3 and Fig. 4 illustrate representative results of SWS map generation in one of the three replicates of acquisitions on the third MH using RSWE without or with gel pad, respectively. The selected ROIs are represented as a dashed white rectangle on each figure. Considering the complex foot structure, all ROIs were manually selected. The ROIs cover the top of the skin to the top of the corresponding anatomical landmark with a width of 2 cm. This depth is approximately 1 cm but may vary per location or volunteer.

Supersonic Imaging

Supersonic imaging (SSI) acquisition was performed at the Centre for Biomechanics and Rehabilitation Technologies Staffordshire University. The same volunteers, with non-substantial weight or BMI changes, lay supine on the couch with their feet positioned at the edge of the bed. The data were acquired using a linear transducer (4–15 MHz, SL 15-4 Linear 140 transducer, SuperSonic Imagine, Aix-en-Provence, France) attached to the ultrasound device Aixplorer (SuperSonic Imagine). In this approach, the SWS corresponds to a group velocity and is performed by using a single push based on acoustic radiation force with a frequency content of the shear wave velocity that increases to a maximum of 500 Hz (Deffieux et al. 2008). The acquisition protocol was performed following the same procedure use for the RSWE experiments. Fig 5, Fig provide examples of the SSI acquisition. The selected ROI is also represented by a *dashed white rectangle*. Previous studies have reported the reliability of SSI in measuring SWS (Lacourpaille et al. 2012). Hence a single measure of SSI was used for the purpose of the study. Finally, the comparison between RSWE (at 500 Hz) and SSI was performed by calculating the elastographic signal-to-noise ratio (SNRe) by dividing the mean by the standard deviation (SD) of each ROI of the SWS map (Ahmed et al. 2018; Ahmed and Doyley 2020).

Statistical Analysis

The coefficient of variation (CV) was calculated by dividing the SD by the average SWS of the three data acquisition values to assess the repeatability of the experiments.

As the CV of the data was not normally distributed (Shapiro–Wilk normality test: p value < 0.05), Friedman's tests were used to assess if CV differs with frequency, use of gel pad and foot side, as well as to identify significant differences in the average SWS between different groups of characteristics. Complementary pairwise Wilcoxon tests with Bonferroni correction were used to

identify which groups had significant differences in CVs between regions. Finally, multiple Spearman's rank-order correlation tests with Bonferroni correction were used to evaluate the relation between the SWSs obtained from RSWE and SSI. All statistical tests were performed using R Statistical Software version 4.0.2 (R Foundation for Statistical Computing, Vienna, Austria).

RESULTS

Fig. 7 compares results of the average SWS obtained in experiments with and without gel pads in all volunteers. Fig. 8 illustrates a representative result of the average SWS of the three trials of the experiments with and without gel pad in one volunteer using the RSWE approach. In addition, Fig. 9, Fig. 10 illustrate the means$\pm$ SD of the three trials at each location for all volunteers without and with gel pad, respectively.

Table 1 outlines the results of the CV by the test–retest experiment. No significant differences were found in CV values for the SWS of RSWE when different frequencies ($p = 0.24$, >0.05) were used. There were no significant differences in CVs for the SWSs of RSWE with and without the gel pad ($p = 0.87$, >0.05). Also, the left and right feet did not significantly differ with respect to the reverberant shear wave speed ($p = 0.14$, >0.05).

There was a significant difference ($p < 0.05$) in CVs between regions. Table 2 outlines the paired comparison of CVs by region. A significant difference can be observed between the heel (median: 9.88%) and the first (median: 5.19%) and third (median: 4.60%) MHs.

Table 3 outlines a significant difference in the mean SWS by frequency ($p < 0.05$). However, when a gel pad was used, no significant difference in measured SWS ($p > 0.05$) or foot

side ($p < 0.05$) was observed. There was a significant difference in the average SWSs ($p < 0.05$) across the volunteers.

Table 4 indicates that there are significant differences between the average SWS of the first MH (median: 2.42 m/s) and those of the third MH (median: 2.16 m/s) and heel (median: 2.03 m/s).

Regarding the comparison against SSI, Fig. 11 illustrates the results of the SWS of one trial of RSWE (at 500 Hz) and SSI without the gel pad. The difference in SWSs is between 0.55 and 4.88 m/s. Similarly, Fig. 12 illustrates the SWSs obtained with the gel pad generating a difference ranging between 2.19 and 4.61 m/s. In Fig. 13 are the results of the SNRe corresponding to the experiments presented in Fig. 11 and 12.

Finally, Table 5 outlines the Spearman correlations between the SWSs obtained with RSWE and SSI. There was a positive correlation with ($p < 0.05$) in the third MH of the right foot ($r = 1$ at 450 Hz) when a gel pad was used. No other significant differences were found.

.

DISCUSSION

This study assesses the feasibility of applying the RSWE approach to mechanical characterization of the plantar soft tissue of the foot. The performed analysis providing encouraging results for the three locations. The CVs of the test–retest analysis revealed a low percentage of variability in all experiments (7.40 ± 5.50 %). Additionally, the CVs for the measured SWSs were not found to differ significantly at each frequency analyzed and between the left and right feet. This indicates that RSWE can be performed with good repeatability..

With respect to the use of gel pads, the CV and average SWS indicated non-significant differences; however, a difference could be observed in the SWS maps in Fig. 3 and 4. In Fig. 3, a representative result of the SWS on the third MH when the gel pad was not used is shown. The presence of artifacts in the SWS generation resulting from the near-field effect of the ultrasound is noted at the top of the image. On the other hand, Fig. 4 illustrates the SWS at the same location from the same volunteer when the gel pad was used. This can indicate that use of the gel pad successfully overcomes the generation of artifacts. Even if surface acoustic waves were generated, the polarization of continuous vibration at a specific frequency generates predominant shear waves in contrast to other effects (Zvietcovich et al. 2019).

The comparison between locations (Table 2) revealed a significant difference between the CV at the heel and those at the first and third MHs. A possible source of error could be that anatomical landmarks of metatarsal heads present a higher contrast with the tissue than anatomical landmarks of the heel, which can be challenging to find by the sonographer considering its heterogeneous mechanical properties. Lin et al. (2015) reported that the success of the acquisition in the heel may depend on the experience and technique of the operator. Considering the average SWS, the three locations differed significantly (Table 4). On average, the lowest and highest values of stiffness were found in the heel (2.03 m/s) and first MH (2.42 m/s), respectively. This is in agreement with results reported in Sun et al. (2011), where the stiffness of plantar soft tissue was analyzed through Young's modulus using an ultrasound palpation system.

Table 3 indicates that the SWS increases significantly at higher frequencies. This trend is consistent with previous work from Pai and Ledoux (2010), in which increasing stiffness was observed when the frequency was increased because of the viscoelastic properties of plantar soft

tissue. This result can be useful in characterizing the relationship between SWS and frequency through analysis of the linear dispersion. Further studies are to be conducted to assess the dispersion caused by using this information.

Considering that the literature on characterization of plantar soft tissue using shear wave elastography is limited, the objective of this work was to compare the results and limitations of the RSWE approach against a commercially available reference such as SSI. Lin et al. (2017a,) reported an SWS analysis on the foot using SSI in the approximate range 1.22–2.78 m/s (calculated based on the reported stiffness) in the heel by taking small circular regions without a gel pad. Additionally, in the work of Wu et al. (2018), a range of 3.09–4.07 m/s was found for the entire heel pad. The selected ROI was a circular ROI that included the microchamber and microchamber layers of the heel pad. In this study, the ROI was a rectangle that included more information than in the previous reports. For that reason, in SSI, the SWS values of the heel are larger than those previously reported. In addition, this difference can be attributed to the fact that this approach has a high probability of generating artifacts in plantar soft tissue caused by boundary effects of the plane shear waves or by the superposition of waves resulting from multiple reflections of foot bones (Deffieux et al. 2011; Lin et al. 2017). In contrast, even when the RSWE approach includes artifacts, the SWS generates results more comparable with the literature. Along the same line, it is noted that SSI generates a lower SNRe (1.77 ± 0.34) than RSWE (5.82 ± 2.19) because of the artifact effect. A potential postprocessing can be performed to overcome this problem; however, in this work, access to the SSI raw data was not available. Further studies can focus on additional processing to enhance the SNRe for this comparison. On the other hand, when a gel pad is used, the SNRe was 6.32 ± 2.47 and 3.72 ± 0.64 for RSWE and SSI, respectively. Both approaches improved the SNRe results, respectively; however, it is important to note that in SSI, while the SD

of the ROI decreases, the average SWS increases. This effect occurs because use of a gel pad generates a bias in the estimation for SSI produced by the wave reflection in the foot. Finally, on the basis of Spearman's test, only one positive, strong correlation was found that could be owing to the previously reported bias and low SNRe from the SSI approach. Additional studies, with postprocessing data are required to verify a more substantial relation between the two approaches.

In general, alternative elastography approaches consider that the shear wave propagation must be in the lateral direction and try to avoid reflections (Parker et al. 2017), which could be challenging because of the complexities of foot anatomy. In that sense, RSWE was used under the assumption that in heterogeneous media, such as in the foot structure, the reflections could benefit the generation of the reverberant field. Hence, this study illustrates the potential of RSWE to adequately quantify foot stiffness through the SWS.

Although the results reveal viscoelastic behavior, an appropriate viscoelastic model needs to be developed in the future. Previous studies (Naemi et al. 2016a, 2016b) established viscoelastic models for foot–ground interaction with a focus on the heel pad. There is a need to develop models that can be applied to metatarsal pads and that consider shear and normal stress.

CONCLUSIONS

This study proves that the RSWE approach can estimate the SWS of the foot in the first MH, third MH and calcaneus in a range between 400 and 600 Hz, providing good repeatability and consistent average SWS estimates. This approach also illustrates that use of a gel pad could be more beneficial in SWS estimation to avoid the presence of artifacts caused by the near-field ultrasound effect. Finally, the RSWE approach has the potential to characterize the mechanical properties of

the plantar soft tissue of the foot, and future studies can investigate the differences between healthy and diseased feet.

Acknowledgments— We are grateful to Elastance Imaging for the loan of the vibration sources equipment. We also thank Dr. Kevin J. Parker for his technical suggestions and advice regarding the Reverberant shear wave elastography approach.

This work was funded by the Binational UK-PERU Newton-Paulet Fund administered by the Fondo Nacional de Desarrollo Cientifico y Tecnologico- PERU under grant 232-2018-FONDECYT from the Peruvian Government. In particular, Stefano Romero was under the doctoral scholarship program in Computer Science (174-2020- FONDECYT- PUCP). In addition, Benjamin Castaneda was supported by the PUCP Research Award Period.

Conflict of interest— The authors declare that they have no conflict of interest.

REFERENCES

Ahmed, R., Gerber, S. A., McAleavey, S. A., Schifitto, G., & Doyley, M. M. Plane-wave imaging improves single-track location shear wave elasticity imaging. IEEE transactions on ultrasonics, ferroelectrics, and frequency control, 2018, 65(8), 1402-1414.

Ahmed, R., & Doyley, M. M. Parallel Receive Beamforming Improves the Performance of Focused Transmit-Based Single-Track Location Shear Wave Elastography. IEEE transactions on ultrasonics, ferroelectrics, and frequency control, 2020, 67(10), 2057-2068.

Cárdenas, M. K., Mirelman, A. J., Galvin, C. J., Lazo-Porras, M., Pinto, M., Miranda, J. J., & Gilman, R. H. The cost of illness attributable to diabetic foot and cost-effectiveness of secondary prevention in Peru. BMC health services research, 2015; 1-10.

Chao CY, Zheng YP, Cheing GL. Epidermal thickness and biomechanical properties of plantar tissues in diabetic foot. Ultrasound in medicine & 201 biology, 2011; 37:1029-1038

Chatzistergos PE, Naemi R, Sundar L, Ramachandran A, Chockalingam N. The relationship between the mechanical properties of heel-pad and common clinical measures associated with foot ulcers in patients with diabetes. Journal of Diabetes and its Complications, 2014;28:488 - 493.

Chatzistergos PE, Behforootan S, Allan D, Naemi R, Chockalingam N. Shear wave elastography can assess the *in-vivo* nonlinear mechanical behavior of heel-pad. J Biomech 2018;80:144–50. doi:10.1016/j.jbiomech.2018.09.003.

Chiu, Y. H., Chang, K. V., Chen, J., Wu, W. T., & Özçakar, L. . Utility of sonoelastography for the evaluation of rotator cuff tendon and pertinent disorders: a systematic review and meta-analysis 2020. European Radiology, 30(12), 6663-6672.

Deffieux, T., Montaldo, G., Tanter, M., & Fink, M. . Shear wave spectroscopy for in vivo quantification of human soft tissues visco-elasticity. IEEE transactions on medical imaging, 2008, 28(3), 313-322.

Deffieux, T., Gennisson, J. L., Bercoff, J., & Tanter, M. . On the effects of reflected waves in transient shear wave elastography. IEEE transactions on ultrasonics, ferroelectrics, and frequency control, 2011, 58(10), 2032-2035.

Flores, G., Ormachea, J., Romero, S. E., Zvietcovich, F., Parker, K. J., & Castaneda, B. Experimental study to evaluate the generation of reverberant shear wave fields (R-SWF) in homogenous media. In 2020 IEEE international ultrasonics symposium (IUS) (pp. 1-4). IEEE.

Gonzalez, E. A., Romero, S. E., Castaneda, B. Real-time crawling wave sonoelastography for human muscle characterization: Initial results. IEEE transactions on ultrasonics, ferroelectrics, and frequency control, 2018, 66(3), 563-571.

Hill, C. L., Gill, T. K., Menz, H. B., & Taylor, A. W. Prevalence and correlates of foot pain in a population-based study: the North West Adelaide health study. Journal of foot and ankle research, 2008, 1(1), 1-7.

Hoyt, K., Kneezel, T., Castaneda, B., & Parker, K. J. Quantitative sonoelastography for the in vivo assessment of skeletal muscle viscoelasticity, 2008. Physics in Medicine & Biology, 53(15), 4063.

Hsu, P. C., Chang, K. V., Wu, W. T., Wang, J. C., & Özçakar, L. Effects of ultrasound-guided peritendinous and intrabursal corticosteroid injections on shoulder tendon elasticity: a post hoc analysis of a randomized controlled trial. Archives of Physical Medicine and Rehabilitation, 2021, 102(5), 905-913.

Klaesner JW, Hastings MK, Zou D, Lewis C, Mueller MJ. Plantar tissue stiffness in patients with diabetes mellitus and peripheral neuropathy. Archives of physical medicine and rehabilitation, 2002;83:1796 - 1801.

Klucinecc, Brian. The effectiveness of the aquaflex gel pad in the transmission of acoustic energy. Journal of athletic training, 1996, vol. 31, no 4, p. 313.

Lacourpaille, L., Hug, F., Bouillard, K., Hogrel, J. Y., & Nordez, A. (2012). Supersonic shear imaging provides a reliable measurement of resting muscle shear elastic modulus. Physiological measurement, 33(3), N19.

Lin C-Y, Chen P-Y, Shau Y-W, Tai H-C, Wang C-L. Spatial-dependent mechanical properties of the heel pad by shear wave elastography. J Biomech 2017;53:191–5. doi:10.1016/j.jbiomech.2017.01.004.

Lin, C. Y., Lin, C. C., Chou, Y. C., Chen, P. Y., & Wang, C. L. Heel pad stiffness in plantar heel pain by shear wave elastography. Ultrasound in medicine & biology, 2015, 41(11), 2890-2898.

Lin, C. Y., Chen, P. Y., Shau, Y. W., & Wang, C. L. . An artifact in supersonic shear wave elastography. Ultrasound in medicine & biology, 2017, 43(2), 517-530.

Loupas, T., Peterson, R. B., & Gill, R. W.. Experimental evaluation of velocity and power estimation for ultrasound blood flow imaging, by means of a two-dimensional autocorrelation approach. IEEE transactions on ultrasonics, ferroelectrics, and frequency control, 1995;42(4), 689-699.

Machado, E., Romero, S. E., Flores, G., Castaneda, B. Feasibility of Reverberant Shear Wave Elastography for In Vivo Assessment of Skeletal Muscle Viscoelasticity. In 2020 IEEE International Ultrasonics Symposium (IUS), 2020 (pp. 1-4).

Naemi R, Chockalingam N. Mathematical models to assess foot-ground interaction: an overview. Med Sci Sports Exerc 2013; 45:1524–33. doi:10.1249/MSS.0b013e31828be3a7.

Naemi R, Chatzistergos P, Sundar L, Chockalingam N, Ramachandran A. Differences in the mechanical characteristics of plantar soft tissue between ulcerated and non-ulcerated foot. Journal of Diabetes and its Complications, 2016a;30:1293-1299.

Naemi R, Chatzistergos PE, Chockalingam N. A mathematical method for quantifying in vivo mechanical behaviour of heel pad under dynamic load. Med Biol Eng Comput 2016b; 54:341–50. doi:10.1007/s11517-015-1316-5

Naemi R, Chatzistergos P, Suresh S, Sundar L, Chockalingam N, Ramachandran A. Can plantar soft tissue mechanics enhance prognosis of diabetic foot ulcer? Diabetes Research and Clinical Practice, 2017;126:182-191.

Ormachea J, Castaneda B, Parker KJ. Shear wave speed estimation using reverberant shear wave fields: implementation and feasibility studies. Ultrasound in medicine & biology, 2018;44:963-977

Pai, Shruti; Ledoux, William R. The compressive mechanical properties of diabetic and non-diabetic plantar soft tissue. Journal of biomechanics, 2010, vol. 43, no 9, p. 1754-1760.

Parker KJ, Doyley MM, Rubens DJ. Imaging the elastic properties of tissue: the 20 year perspective. Physics in medicine & biology, 2011;56:R1.

Parker, K. J., Ormachea, J., Zvietcovich, F., & Castaneda, B. (2017). Reverberant shear wave fields and estimation of tissue properties. Physics in Medicine & Biology, 62(3), 1046.

Pendsey SP. Understanding diabetic foot. International journal of diabetes in developing countries, 2010;30:75.

Sigrist RM, Liau J, El Ka as A, Chammas MC, Willmann JK. Ultrasound elastography: review of techniques and clinical applications. Theranostics, 2017;7:1303.

Sun, J. H., Cheng, B. K., Zheng, Y. P., Huang, Y. P., Leung, J. Y., & Cheing, G. L. . Changes in the thickness and stiffness of plantar soft tissues in people with diabetic peripheral neuropathy. Archives of physical medicine and rehabilitation, 92(9), 2011; 1484-1489.

Wu C-H, Lin C-Y, Hsiao M-Y, Cheng Y-H, Chen W-S, Wang T-G. Altered stiffness of microchamber and macrochamber layers in the aged heel pad: Shear wave ultrasound elastography evaluation. J Formos Med Assoc 2018;117:434–9. doi:10.1016/J.JFMA.2017.05.006.

Yablon, C. M. Ultrasound-guided interventions of the foot and ankle. In Seminars in musculoskeletal radiology (Vol. 17, No. 01, pp. 060-068, 2013). Thieme Medical Publishers.

Zvietcovich F, Pongchalee P, Meemon P, Rolland JP, Parker KJ. Reverberant 3D optical coherence elastography maps the elasticity of individual corneal layers. Nature Communications, 2019;10:1-13.

FIGURES

Fig. 1. Positions of the transducer to acquire the first metatarsal head (a), the third metatarsal head (b) and the heel (c).

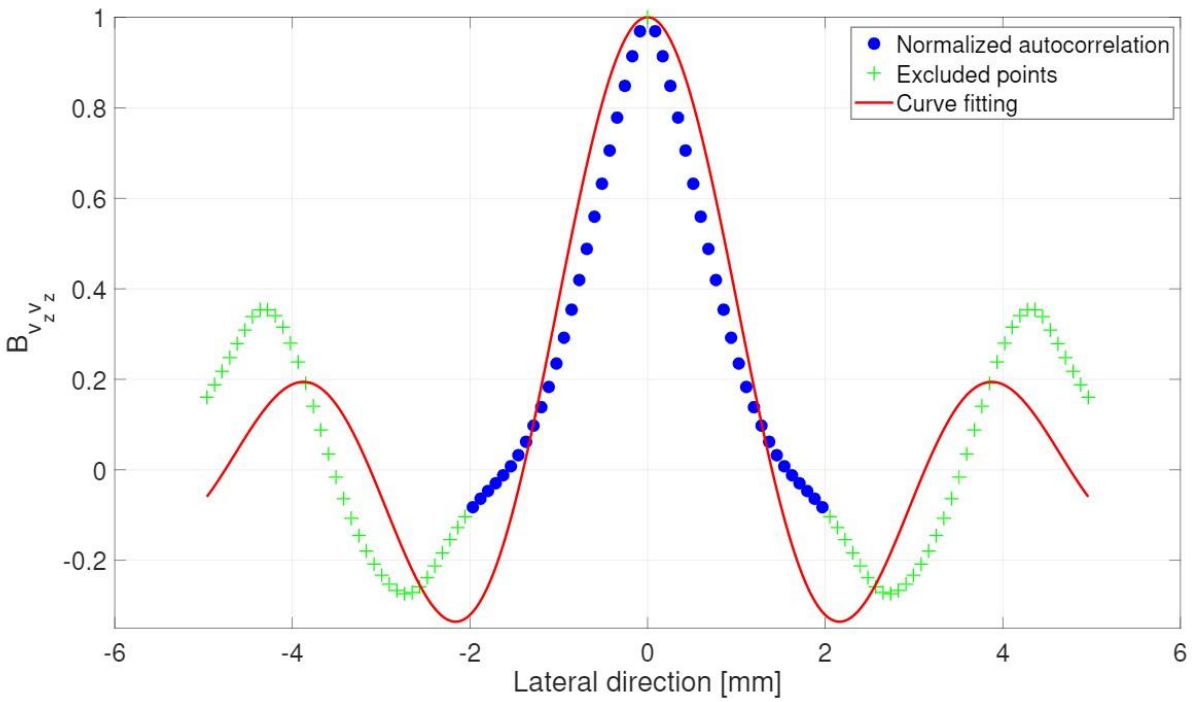

Fig. 2. Curve fitting from the lateral profile from the normalized 2-D autocorrelation.

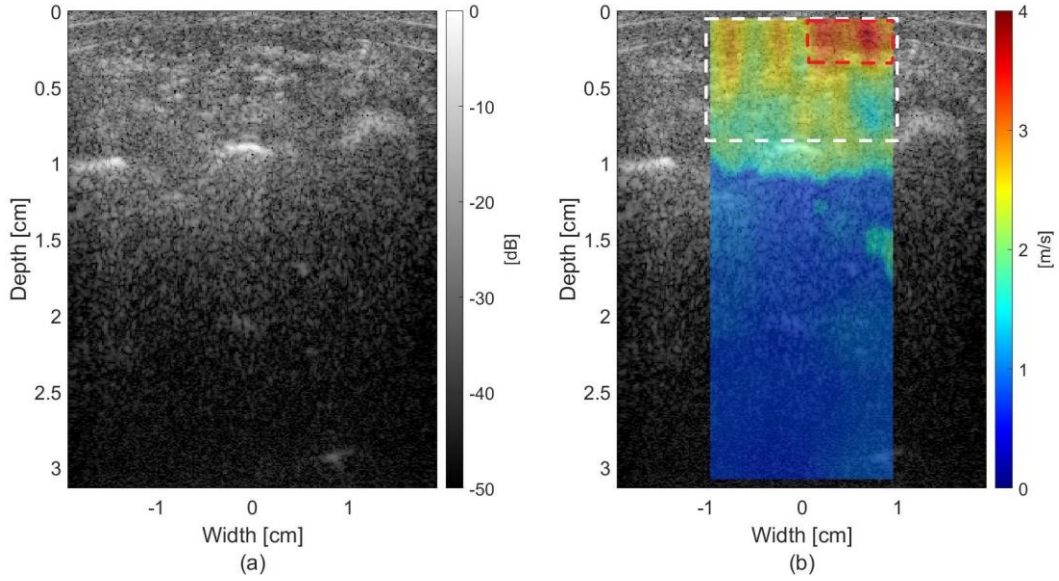

Fig. 3. Representative examples of the third metatarsal head acquisition: (a) B-mode, (b) overlapped reverberant shear wave elastography–shear wave speed map. At a depth below the anatomical landmark, the ultrasound beam wave propagation is lost, then the estimator generates an approximate value of 0 on the shear wave speed map. The analyzed region of interest is represented as the dashed white rectangle, and the generated artefacts, as a dashed red rectangle.

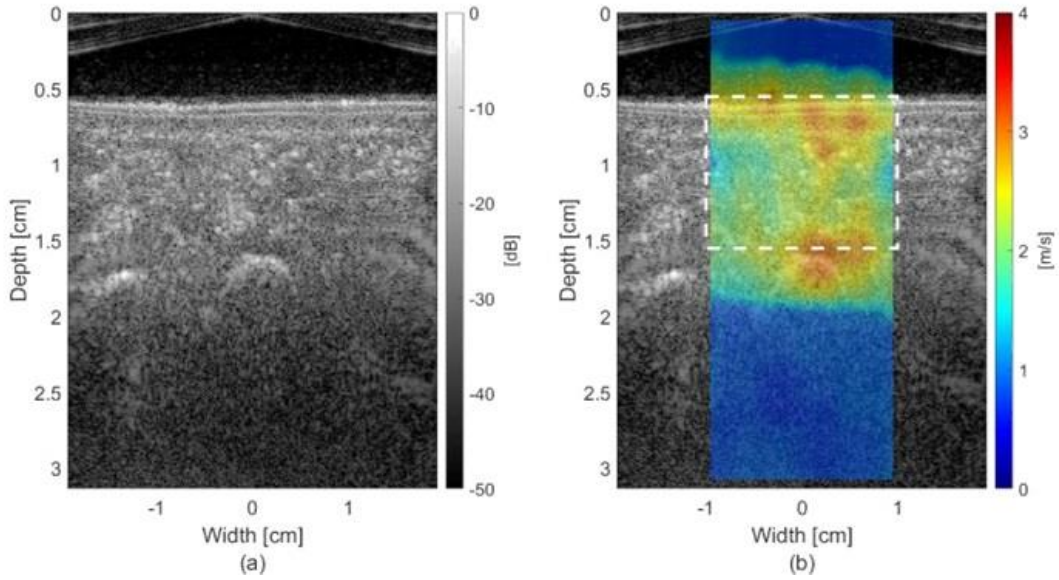

Fig. 4. Representative example of the third metatarsal head acquisition using gel pad: (a) B-mode, (b) overlapped reverberant shear wave elastography–shear wave speed map. At a depth below the anatomical landmark, the ultrasound beam wave propagation is lost, then the estimator generates an approximate value of 0 on the shear wave speed map. Therefore, only the region of interest (dashed white rectangle) is taken.

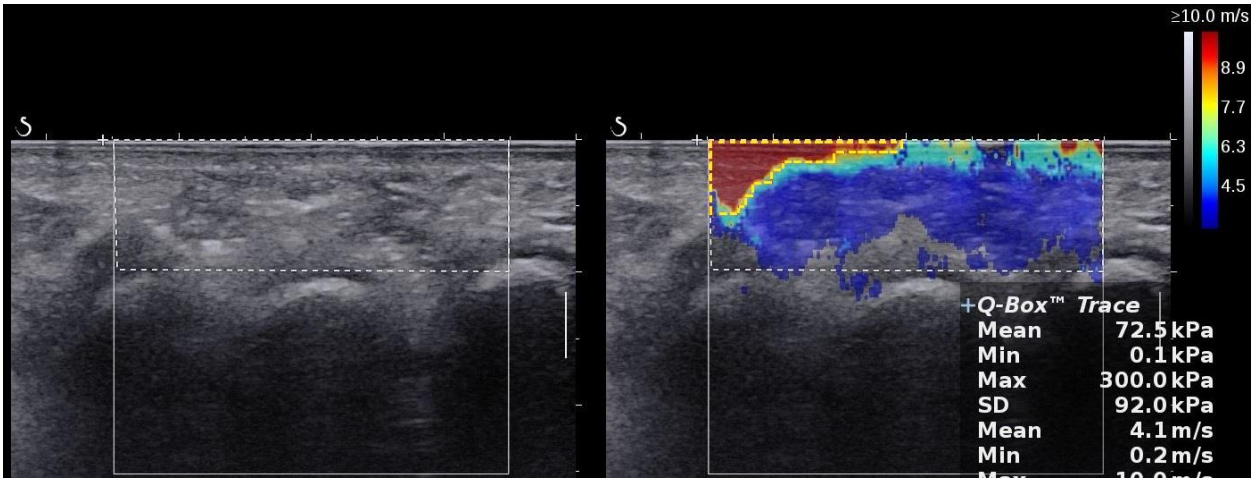

Fig. 5. B-Mode (left) and overlapped supersonic imaging–shear wave speed (right) map from the third metatarsal head indicating the analyzed region of interest (dashed white rectangle) and artefacts (dashed yellow region).

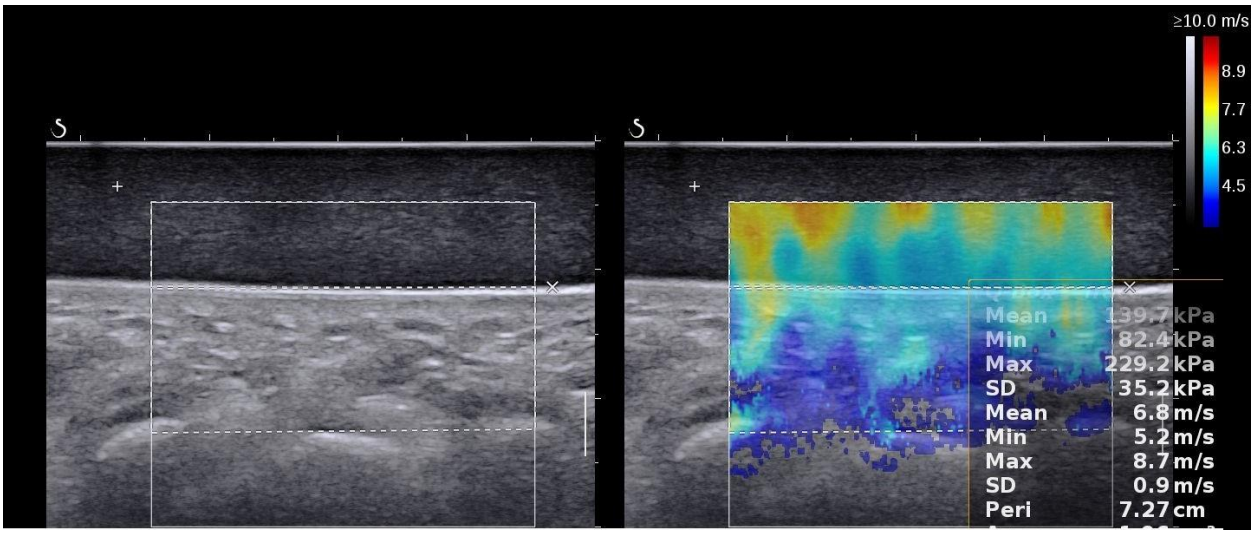

Fig. 6. B-Mode (left) and overlapped supersonic imaging-shear wave speed (right) map from the third metatarsal head acquisition using gel pad material indicating the analyzed region of interest (dashed white rectangle).

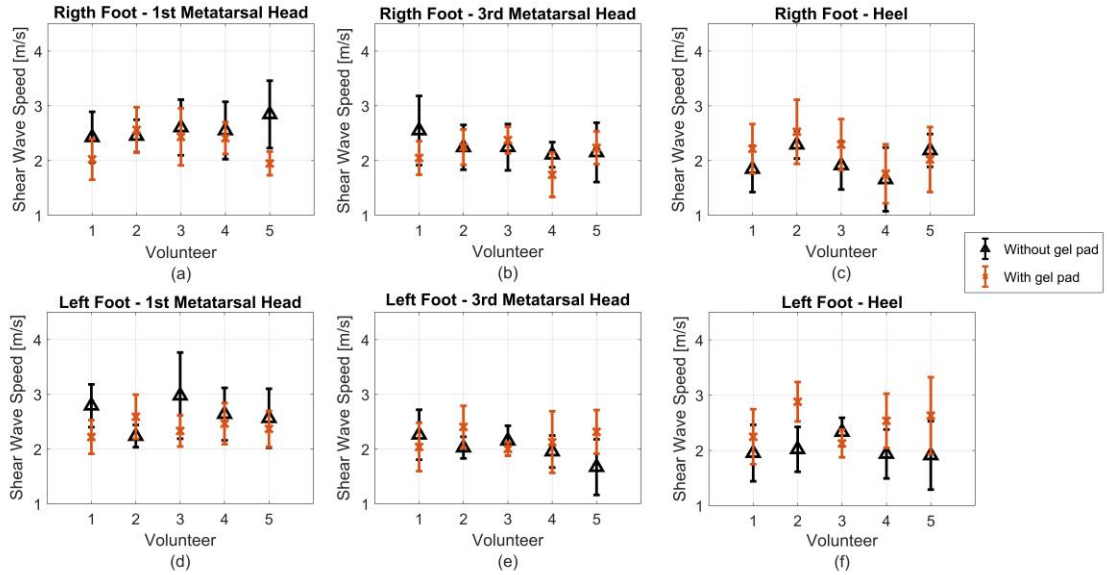

Fig. 7. Comparison between the means ± standard deviations of the shear wave speeds for all volunteers at a frequency of 500 Hz in the (a) right foot, first metatarsal head; (b) right foot, third metatarsal head; (c) right foot, heel; (d) left foot, first metatarsal head; (e) left foot, third metatarsal head; and (f) left foot, heel.

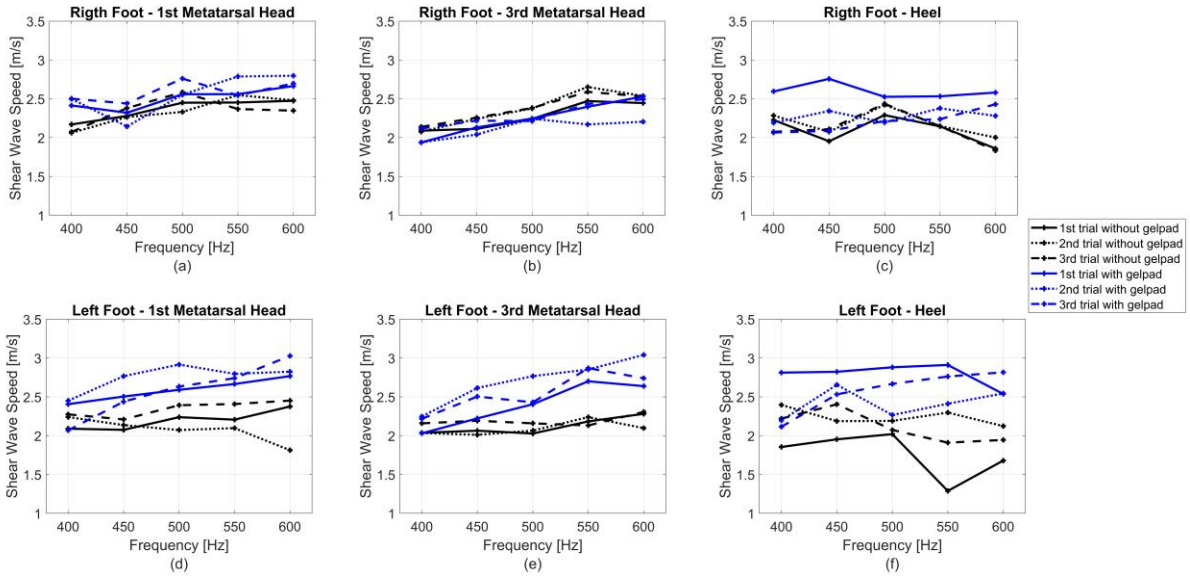

Fig. 8. Mean shear wave speeds for all trials (with and without gel pad) of one volunteer in each location: (a) right foot, first metatarsal head; (b) right foot, third metatarsal head; (c) right foot, heel; (d) left foot, first metatarsal head; (e) left foot, third metatarsal head; and (f) left foot, heel.

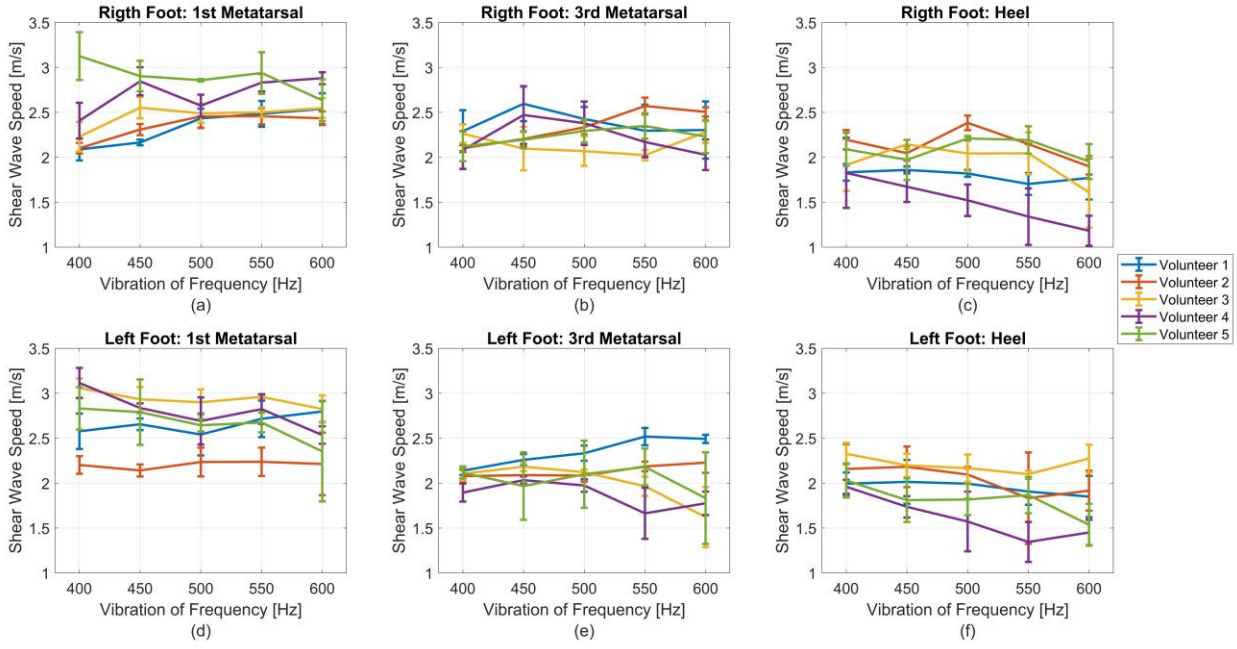

Fig. 9. Means $\pm$ standard deviations of the shear wave speeds of the trials for all the volunteers without using gel pad in each location: (a) right foot, first metatarsal head; (b) right foot, third metatarsal head; (c) right foot, heel; (d) left foot, first metatarsal head; (e) left foot, third metatarsal head; and (f) left foot, heel.

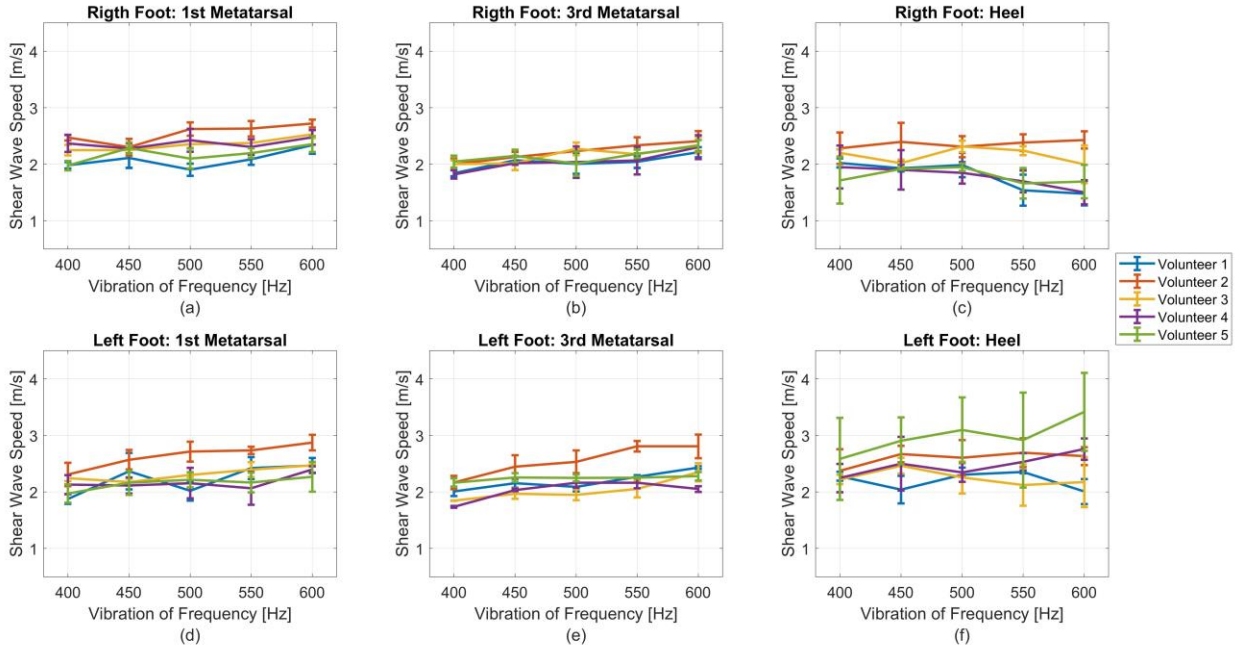

Fig. 10. Means ± standard deviations of the shear wave speeds of the trials for all the volunteers using gel pad in each location: (a) right foot, first metatarsal head; (b) right foot, third metatarsal head; (c) right foot, heel; (d) left foot, first metatarsal head; (e) left foot, third metatarsal head; and (f) left foot, heel.

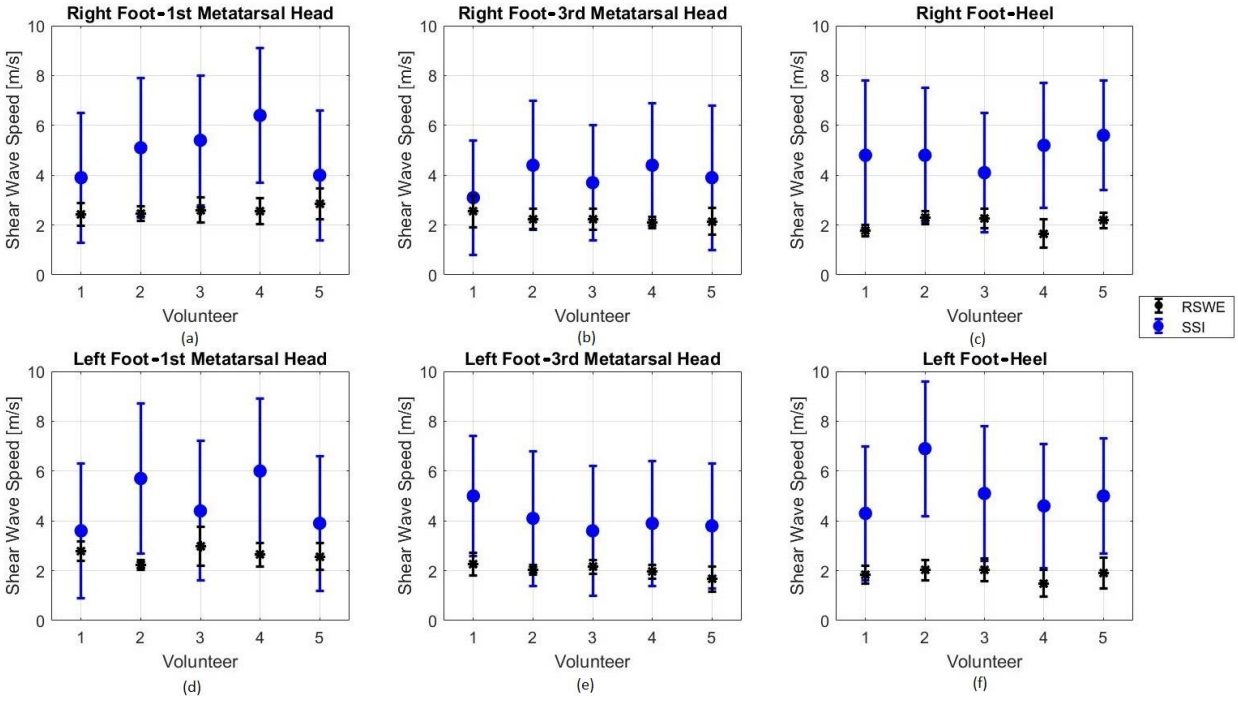

Fig. 11: Comparison between the mean ± standard deviations of the shear wave speeds from reverberant shear wave elastography and supersonic imaging of all volunteers without gel pad. Specific results at 500 Hz applied to the (a) right foot, first metatarsal head; (b) right foot, third metatarsal head; (c) right foot, heel; (d) left foot, first metatarsal head; (e) left foot, third metatarsal head; and (f) left foot, heel.

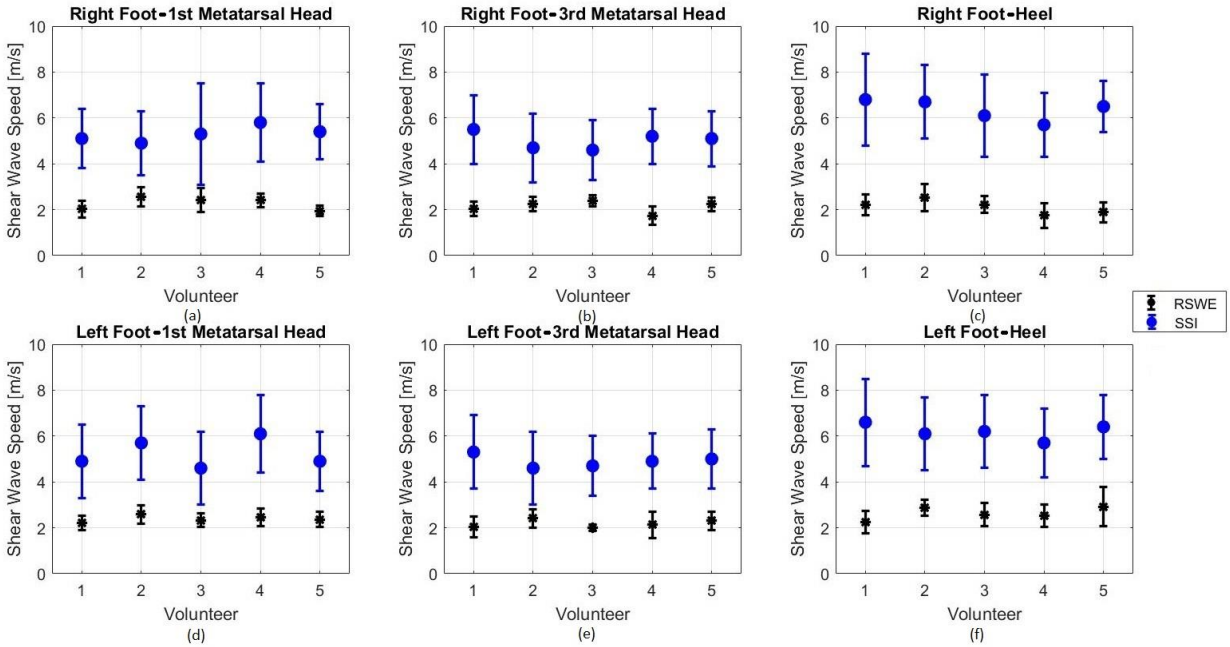

Fig. 12: Comparison between the mean $\pm$ standard deviations of the shear wave speeds from reverberant shear wave elastography and supersonic imaging of all volunteers with gel pad. Specific results at 500 Hz applied to the (a) right foot, first metatarsal head; (b) right foot, third metatarsal head; (c) right foot heel; (d) left foot, first metatarsal head; (e) left foot, third metatarsal head; and (f) left foot, heel

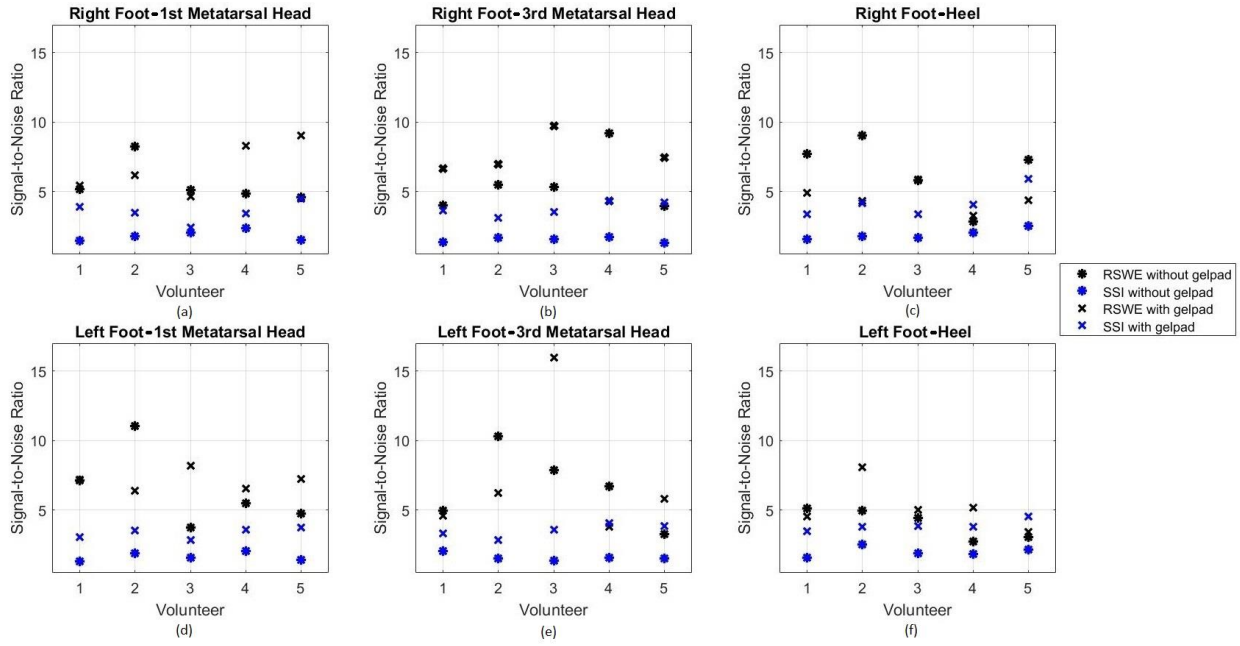

Fig. 13. Comparison between the elastographic signal-to-noise ratio from reverberant shear wave elastography (at 500 Hz) and supersonic imaging of all volunteers with and without gel pad applied to the (a) right foot, first metatarsal head; (b) right foot, third metatarsal head; (c) right foot, heel; (d) left foot, first metatarsal head; (e) left foot, third metatarsal head; and (f) left foot, heel.

Tables

Table 1. Results of Friedman tests of the coefficients of variation of the reverberant shear wave speed approach of the three trails controlling the frequency, the use of gel pad and the foot side

Coefficient of Variation	Median (%)	P-value (no. of observations)
Frequency (Hz)		0.24(300)
400	5.20	
450	4.494	
500	5.634	
550	6.044	
600	6.834	
Use of gel pad		0.87(300)
Without gel pad	5.8323	
With gel pad	5.5952	
Foot side		0.14(300)
Right	5.49	
Left	6.03	

Table 2. Results of the paired Wilcoxon tests with Bonferroni correction of the coefficients of variation of reverberant shear wave speeds between regions

	1st MH	**3rd MH**
3rd MH	1.00(100)	-
Heel	**p<0.05** (100)	**p<0.05** (100)

Table 3. Results from the Friedman's tests of the shear wave speeds of reverberant shear wave speeds controlling the frequency, the use of gel pad and the foot side

	Median of the average SWS (m/s)	P-value (no. of observations)
Frequency (Hz)		**p<0.05(300)**
400	2.12	
450	2.17	
500	2.24	
550	2.22	
600	2.31	
Use of gel pad		0.41 (300)
Without gel pad	2.18	
With gel pad	2.24	
Foot side		0.10(300)
Right	2.19	
Left	2.21	

Table 4. Results from the paired Wilcoxon tests with Bonferroni correction of the shear wave speeds of reverberant shear wave speeds between regions

	1st MH	**3rd MH**
3rd MH	**p<0.05 (100)**	**-**
Heel	**p<0.05 (100)**	**p<0.05 (100)**

Table 5. Spearman's rank correlation coefficients at different frequencies, locations and foot sides with and without gel pad for the shear wave speeds obtained with shear wave elastography and supersonic imaging

		Left Foot			Right Foot		
Use of gel pad	**Frequencies**	**1st**	**3rd**	**Heel**	**1st**	**3rd**	**Heel**
Without	400	-0.05	0.20	-0.46	-0.30	-0.6	-0.10
	450	0.80	0.20	-0.60	0.30	-0.41	0.30
	500	0.40	0.67	0.50	0.60	0.16	0.46
	550	0.21	0.87	0.05	0.10	-0.10	0.3
	600	0.41	0.10	-0.20	-0.20	-0.90	-0.7
With	400	-0.50	-0.70	0.60	0.60	-0.41	-0.05
	450	-0.72	-0.82	0.60	0.80	**1.00(*)**	-0.1
	500	0.36	-0.53	0.70	0.70	0.90	0.2
	550	0.10	0.30	0.82	0.56	0.90	0.46
	600	-0.20	-0.60	-0.67	-0.36	0.05	0.20

(*) p<0.05

1